In silico Insights on the Allosteric Modulation of the μ-Opioid Receptor and G protein Complex in the Presence of Agonist Ligand BU72 and Potential Positive Allosteric Modulator BMS-986121

Mac Kevin E. Braza and Ricky B. Nellas*

Institute of Chemistry, College of Science, University of the Philippines Diliman, Quezon City, 1101, Philippines

E-mail: rbnellas@up.edu.ph

Abstract

The G protein-coupled receptor (GPCR) μ-opioid receptor (μOR) is one of several drug targets of commercially available therapeutics for pain. Various opioid drugs like morphines have been associated to numerous substance abuse-related deaths around the world. A better alternative to avoid this undesirable side effect is by targeting allosteric sites. In addition, understanding the underlying mechanism of allosteric ligands in μOR is highly sought for better drug optimizations. Using molecular dynamics, the allosteric behavior of the μOR and G protein complex in the presence of agonist ligand BU72 and potential positive allosteric modulator (PAM) BMS-986121 was probed by observing residue-residue contacts formation and breakage. It was found that G protein residues D959, L349, and K963 participate in the interprotein contact formation

between μOR and G protein. Moreover, orthosteric binding site residues D83, Y84, and H233 polar interactions were verified to be critical not only on the agonist ligand binding, but also in the allosteric communication of the protein complex. Also, the overall decrease on the number of contacts was observed after mutations, which can trigger the opening of the orthosteric binding site. Rationalization of allosteric modulation in μ-opioid receptor-G protein complex may improve drug discovery schemes and strategies for allosteric drugs including other targets in the GPCR protein families.

Keywords

μ-Opioid receptor, G protein, molecular dynamics simulations, allosteric regulations, principal component analysis, CAMERRA

1 Introduction

The G protein-coupled receptors (GPCR) signal transduction is intrinsically allosteric in nature.(*1*) Allosterism is defined as a process in which the effect of ligand binding is transmitted to distal and functional sites and to the regulation of protein's physiological activity.(*2*) Here, the binding of external signals, such as ions, hormones, neurotransmitters, and ligands to GPCRs transmits a communication to another spatially distant protein (e.g. G proteins and β-arrestin). The participation of these GPCRs in numerous physiological functions highlights their vital role as a drug target for almost 30% of commercial drugs.(*3*) In addition, several drug discovery schemes have focused on the allosteric modulations of GPCR because of its higher selectivity, potency, and safety.(*1*, *4*–*6*)

The μ-opioid receptor (μOR) is a class A G protein-coupled receptor (GPCR) that is a target of therapeutic opioid drugs for acute and chronic pains.(*5*, *7*) The function of opioid receptors includes regulation of membrane ionic homeostasis, emotional response, respiratory and cardiovascular control, etc.(*8*) Studies have shown that μOR is also responsible for the

drug addiction behaviors which are believed to be an agonist-driven process.(*9*) Moreover, targeting μOR with drugs that can induce analgesia via signaling through G protein G_i pathway is highly sought.(*10*) This is in contrast with β-arrestin signaling pathway that is known to be connected with lethal side effects (e.g. respiratory depression, addiction, and tolerance).(*11–13*)

The binding of ligands to μOR causes structural changes from the helices to the loops in the cell membrane, eliciting an intracellular response.(*14*) The canonical active state of μOR is obtained after the binding of agonist to the orthosteric binding site resulting in the rearrangement of transmembrane (TM) helices TM5, TM6, and TM7.(*15*, *16*) Following the rearrangement is the binding of G proteins to the activated μOR.(*17–19*) On the other hand, Protein Data Bank (PDB) has records of various activated- and inactivated-μOR structures.(*15*, *20*) Despite of their complexities, recent developments in molecular engineering, X-ray crystallography, and cryo-electron microscopy have allowed the full elucidation of μOR-G protein complex.(*16*) This recently-resolved structure of μOR-G protein complex by Koehl et al. is an important breakthrough for the structural and dynamics basis of GPCR-G protein signaling.(*16*)

For years, combinations of modeling and pharmacological techniques allowed the discovery of the novel inhibitors.(*21*, *22*) However, both experimental and modeling studies on μOR are limited to the spatial and temporal resolutions of the methods employed. Molecular dynamics (MD) simulations can represent all-atom model of a protein in high resolutions while different perturbations can be easily manipulated.(*23*) Computer simulations showed that the motions leading to the allosteric network are loosely coupled and connect small changes at the extracellular orthosteric sites and at the intracellular G protein binding site. (*24*, *25*) Since the μOR-G protein complex was recently resolved, it is expected to have an increase in various modeling studies that will utilize the structure. In addition, the MD simulations of individual mutants are valuable in the understanding of the internal dynamic changes in the protein.(*26*) Although long microsecond simulations are achievable

with supercomputers, such level is still beyond reach, especially with membrane proteins, like GPCR. Furthermore, our motivation to analyze short all-atom 30-ns MD simulations is to set-up basis on the systematic monitoring of mutational phenotypic effects in μ-OR allosteric dynamics. Moreover, the early signaling effects are important trigger for the activation process especially in GPCR. To the best of our knowledge, our work presents the first repeat to investigate the allosteric modulation in both μOR and G protein complex.(*21*)

Here, we seek to identify the structural and dynamics effect of a potential positive allosteric modulator, BMS-986121, to the μ-opioid receptor-G protein complex with BU72 and measure the effect of orthosteric binding site residues to the overall dynamics of the complex by employing glycine-mutation scanning. MD simulations were done to generate a set of conformations of the μOR-G protein complex. To probe the allosteric nature of the μOR, "Computation of Allosteric Mechanism by Evaluating Residue-Residue Associations" (CAMERRA) tool was used to analyze the dynamics of the residue-residue contact formation and breakage. Also, different glycine mutants of μOR were generated to determine the nature of the interaction between the agonist and the orthosteric binding site and their effect to the coupling dynamics. The structural dynamics and the basis for allosteric modulation in μOR with PAM may be elucidated here.

2 Results and Discussion

The identification of structural and dynamics bases of allosteric regulation is crucial for the rational design of potential pain therapeutics. Here, we applied the analysis of correlated residue-residue contacts breaking and forming in structures obtained from 30-ns all-atom MD simulations of the whole μOR-G protein complex in an explicit aqueous POPC lipid bilayer. The CAMERRA method was proven to be useful in mapping allostery in membrane protein. It also revealed critical residues in accordance with the resolved μ-OR structures.

2.1 Molecular docking

Probable allosteric binding sites for the μOR were determined using molecular docking in AutoDock Vina (Figure 1).(*27*) Binding pockets for agonist ligand BU72 and allosteric ligand BMS-986121 are illustrated. These were based on the most favorable binding pose and sites for each ligand (i.e. lowest binding energy).

As starting point for MD simulations, the highest binding affinity of ligand pose was chosen. To verify, an ensemble blind docking for the whole μOR was performed. MD-derived structures from the 30-ns μ-OR-BU72 simulations were used. The three most populated clusters show similar amino acid residues for BMS-986121 binding site (SI Figure 1). Furthermore, the average binding energy calculated was -7.5 $\pm$ -0.55 kcal·mol^{-1}. BU72 and BMS-986121 ligands' RMSD were reported (SI Figure 2) to be stable in their sites. Overall, the binding pose for the ligand was characterized with RMSD values $<$ 2.5 Å relative to the first frame (i.e. docking pose).

Buprenorphine BU72, a synthetic bridged-pyrrolidinomorphinan, is an agonist of μOR.(*15*, *28*, *28*) It was found to be a very potent respiratory depressing drug to nonhuman primates.(*28*, *29*) The reported crystal structure of BU72-bound μOR is observed to have the same binding pose as the antagonist β-funaltrexamine (β-FNA) in μOR.(*15*, *20*) In addition, morphinan scaffold is responsible for the similar binding orientation of the two drugs.

We used the potential positive allosteric modulator (PAM) BMS-986121 as a target ligand.(*30*, *31*) This PAM is a thiazol-2-amine analogue [(4-{2-[(2,6-dichlorophenyl)amino]-1,3-thiazol-4-yl}phenyl)(hydroxy)imino]-λ1-oxidanyl that increases the potency of [D-Ala^2, N-MePhe^4, Gly-ol]-enkephalin (DAMGO) when bound to μOR. The increase in cooperativity factor (α) by 7 is an indication of a positive allostery.(*31*, *32*) Also, this was linked to the G protein activation in [^{35}S]GTPγS-binding studies in membranes.

Unlike the agonist ligand, structural data for the allosteric binding sites of μOR are yet to be resolved. In the advent of the success of molecular docking algorithms in predicting binding site, this method can provide information on probable allosteric ligand's pose and

binding pockets. We applied ensemble blind docking and use the lowest binding energy pose (i.e. most stable) in the MD simulations. Blind docking is a method in which the binding site is not assumed, in contrast to resolved binding site structures.(*33*) We verified the reproducibility of the BMS-986121 binding pose. The stabilizing force of BMS-986121 binding is characterized by hydrophobic interactions. On the other hand, the binding site for the agonist ligand BU72 was verified and confirmed to be in agreement with the available crystal and cryo-electron microscopy-resolved structures.(*15*, *16*, *20*) Close interacting residues in the agonist BU72 ligand binding pocket were also determined and used as the basis for single-point glycine mutation scanning.

2.2 Residue-residue contacts analysis

The starting structure of subsequent MD simulations was based on the orientation of the μOR in POPC lipid bilayer (Figure 2). After obtaining the binding pose of each ligand in the μOR, individual MD simulations of complexes were performed. Trajectories were used to extract contact information from each protein-ligand complex. Here, the CAMERRA code was used to calculate and identify dynamic residue-residue contacts.(*34*) After diagonalization, principal components (PC) were obtained. PC corresponds to the vibrational mode of contacts formation (positive) and breaking (negative).(*35*) The workflow for the CAMERRA method is presented in Figure 3 as adapted from the work of Johnson, et al.(*34*) Contacts' normalized eigenvector is represented by colors blue and red, with blue representing a positive correlation and red a negative correlation (Figure 4).

The sum of ligand's PC 1 is presented in Figure 5. Same signs (both positive or both negative) of PC indicate that they are cooperatively engaging while opposite signs indicate negative cooperativity.(*34*, *36*) The positive allosteric modulator showed positive correlations, i.e. cooperative binding, with the agonist BU72 with respect to PC 1. This can explain how allosteric ligands affect BU72 binding more favorable. Also, this can be visualized by using the obtained PC values and projecting them to the μOR structure.

In Figure 5, it can be seen that the interface between the μOR and α1-G protein shows significant contact dynamics. For instance, the α1-G protein shows the most evident effect of allosteric ligand binding. It is known that α1-G protein tends to dissociate after GPCR activation.(*37*, *38*) The observed PAM-protein complex contacts (Figure 6) have positive eigenvector between residue G348 (α1-G protein)-D959 (μOR), and negative eigenvector between residues L349 (α1-G protein)-K963(μOR). In turn, this can lead to the complete rearrangement of the domains within G protein that can also trigger dissociation of the β1- and γ1-subunits.

The projection of PC 1 and PC 2 on the whole PAM-μOR-G protein complex were also done in Figures 7 and 8, respectively. The residue-residue contacts PC is represented by colors blue and red, as well. It can be inferred that although ligands are found in the μOR, majority of the contacts being formed and broken are in G proteins. We found that residues D959, L349, and K963, in Figure 6, contribute to the contact formation of μOR and α1 G protein with PAM BMS-986121 complex. This supports the idea that the concerted motions of amino acid residues can give way to the transmission of signal to the other parts of protein complex.

2.3 Orthosteric binding site probing

We also examined the effects of single-point mutations in orthosteric binding site to the overall dynamics of the complex. Based from agonist binding site in the resolved cryo-EM structure, 17 μOR glycine mutants were also parameterized, simulated, and analyzed.(*16*) In Figure 9, average contacts per residue versus J_{50} of each mutant is presented. J_{50} is defined as the number of contacts that formed $\geq$50% in the whole sampled configuration. The purpose for using J_{50} is to assess the number of dynamic contacts. In contrast, contacts that are formed $\geq$80% and $\leq$20% of the total time represent static contacts that are always present and always absent, respectively.

It was observed that when the contacts per residue increase the average number of con-

tacts of the whole protein also increase. Interestingly, when the side chain was removed in the orthosteric binding sites, the number of contacts was found to decrease, except in V79G. A decrease in the number of contacts implies a less compact protein complex structure, triggering the opening of the orthosteric binding site.

Computational glycine scanning was used in this study. Here, amino acid residues at the agonist binding site was replaced with a glycine residue to identify the effect in the allosteric communication in μOR. In contrast with alanine scanning, glycine scanning can repress the direct protein-ligand interactions and will therefore perturb residue-ligand level contacts.(*35*) Also, nonpolar aliphatic residues (e.g. valine and leucine) may have less to no effect when substituted with alanine instead of glycine (i.e. conservative replacement). Lastly, the removal of secondary architecture (specifically α-helices) by adding glycine can reduce the effect of ligand binding due to this protein's feature.

The overall configuration of each mutant is summarized in Figure 10. Mutant's PC points are colored according to their PC 2 values, positive (blue) and negative (red). Here, we can compare if the mutations are critical to the residue-residue contacts and/or allosteric behavior of μOR as previously done.(*35*) In summary, PC 1 values range from -10 to 10 for all the mutants. Some mutants were observed to have similar positive PC 2 values to the Native (Table 1). These include W69G, V79G, I80G, T154G, V172G, I232G, V236G, W254G, and Y262G. Differences with the Native μOR lie on the PC 2 values of mutants F59G, Q60G, D83G, Y84G, M87G, L155G, H233G, and I258G. We believe that this is the first attempt to analyze the importance of the orthosteric binding site in the context of its role to the allosteric regulations of μOR.

Moreover, our results showed agreement with experimental data of μOR structures and dynamics. For instance, in the reported crystal structure of BU72-bound μOR (PDB ID 5C1M), several residues participated in the polar interactions of the agonist (Table 2). D83 has an ionic interaction with the BU72 tertiary amine.(*15*) Y84 was involved in the extended water-mediated interactions in the active state. Y262 phenolic hydroxyl group interacts with

the BU72 tertiary amine.(*15*) While, H233 is mediated with water when interacting with BU72.(*15*) After the mutation, we have seen that the PC 2 values of these residues had shifted negatively, except in Y262G. Other non-polar interactions are summarized in Table 3.

Our work describes the existence of a network of adjacent residues that connects the orthosteric site with the cytoplasmic surface. We determined that after agonist ligand activation of μOR and allosteric ligand binding, subtle movements in the structure amplify larger conformational change to the cytoplasmic region and to the G proteins.(*39*) Moreover, it is known that the active conformation of GPCR (e.g. μOR) is suggested to be triggered by a two-way allosteric coupling from agonist binding pocket and G protein-coupling interface.(*40*) Here, the agonist binding to GPCR does not only promote binding of G protein to the receptor, but the affinity of agonist is also improved after G protein binding.(*39*) This suggests the bidirectionality of protein allostery.(*41*)

Furthermore, allosteric drugs can change receptors' conformations via two (2) different processes: (1) modulate signal directly; or (2) change the affinity and/or efficacy of orthosteric ligand. In this study, we found that a potential PAM shows subtle changes on the affinity of agonist BU72. Recent work on GPCR simulations showed that allosteric communication is also responsible for transitions of inactive, intermediate, and active states.(*42*, *43*) However, our simulations focus only on the signaling features at the residue level. Here, they can be affected by the allosteric ligand binding and the intracellular G protein coupling. The binding of potential PAM BMS-986121 can therefore prevent μOR down-regulation and other mechanisms (e.g. G protein signaling) triggered by receptor activation produced by agonist BU72 alone. This allosteric ligand, in turn, could lead to less tolerance and dependence than the regulated opioid drugs.(*31*) Spectroscopic studies (e.g. NMR, DEER, and fluorescence spectroscopies) of G protein-binding to the μOR intracellular face can provide additional evidence of the effects of allosteric ligand binding.

To conclude, we presented the application and the analysis of correlated residue-residue

contacts in the μOR that can reveal important insights on the protein complex allosteric communication. Although limited, the perturbation scheme provided aims to generate a set of diverse structures and not necessarily a fully equilibrated ensembles. Moreover, the computational workflow applied in this study can be further improved by considering other GPCR complexities (i.e. water-mediated interactions, allosteric sodium and potassium ions probing, β-arrestin binding, and active-to-inactive state simulations). Our schemes and analysis can provide basis on the systematic monitoring of mutational effects in μOR allosteric communication.

3 Methods

3.1 Systems

The cryo-electron microscope-resolved structure of μ-opioid receptor-G protein complex was retrieved from RCSB Protein Data Bank (PDB ID 6DDE).(*16*) Seventeen (17) glycine mutants of μOR, directed at the orthosteric binding site, were generated: F59G, Q60G, W69G, V79G, I80G, D83G, Y84G, M87G, T154G, L155G, V172G, I232G, H233G, V236G, W254G, I258G, Y262G.

3.2 Molecular dynamics simulations

All-atom MD simulations were performed using NAMD 2.11.(*44*) Initially, the μOR was embedded to 1-palmitoyl-2-oleoyl-sn-glycero-3-phosphocholine (POPC) using OPM and CHARMM-GUI web servers.(*45*, *46*) The AMBER Tools tleap was used for the parameterization of the systems.(*47*) The force fields ff14SB(*48*), TIP3P(*49*), Lipid14(*50*), and GAFF(*51*) for protein, water, lipids, and organic molecules, respectively, were used. Parameters for ligands, BU72 and BMS-986121, were generated using antechamber.(*52*) AMBER's tleap module was used to prepare all glycine mutants.(*47*) For all the systems, minimization, heating, and equilibration were done. Minimization was done for 2 ns (10^4 NPT steps) at 310 K and

1.01325 bar (1.00 atm) to remove bad contacts. Minimization was done for 10,000 steps followed by heating from 0 to 310 K with 5 K increment per step. Particle mesh Ewald with periodic boundary conditions was used for the calculation of electrostatic interactions(*53*) and Langevin dynamics was applied for temperature control at 310 K.(*54*) All systems were subjected in 4 x 250,000 steps sequential equilibration using NPT ensemble (310 K, 1 atm).(*55*, *56*) The total equilibration time for each system was 2 ns. These were followed by a 30-ns NPT production runs at constant room temperature and pressure (310 K and 1 atm). Dataframes were collected at 2 fs interval for the whole 30 ns production run. Trajectories obtained during the production runs were checked using the protein's backbone and ligands' RMSD (SI Figure 2).

3.3 Molecular Docking

An ensemble blind docking was employed using AutoDock VINA.(*27*) Initially, μ-OR - G protein complex with bound BU72 was simulated. An ensemble of structures from the 30-ns all-atom MD simulations was obtained using DBSCAN (density-based) clustering algorithm in AMBER tools cpptraj.(*57*) We used a search space size 60 x 50 x 80 Å centered in the μOR. A search exhaustiveness equals to 50 was used. Then, the lowest binding affinity ligand pose was used for the subsequent MD simulations of PAM-μOR-G protein complexes.

3.4 CAMERRA

Simulation snapshots were obtained from the trajectories generated from MD simulations. These snapshots were used in the "Computation of Allosteric Mechanism by Evaluating Residue-Residue Associations " (CAMERRA). CAMERRA tool was downloaded from http://shenlab.utk.edu/camerra.html.(*34*) Here, the dynamic contacts were determined using the optimum distance cutoff $x = 4.2$ Å. The first step in CAMERRA code is to evaluate all residue-residue contacts. Whereas, the score u_{ij}

$$u_{ij} = \begin{cases} 1, & \text{if } x \leq 4.2\text{Å} \\ 0, & \text{otherwise} \end{cases} \tag{1}$$

Based on this criterion, dynamic contacts (i.e. those contacts that form between 20 to 80 % of the total number of contacts) were obtained. The dynamic contacts were selected and subsequent statistical analysis were done such as obtaining the covariance matrix, diagonalization, and principal component analysis (PCA). Covariance matrix of formation and breaking of contacts were calculated to extract respective eigenvectors and eigenvalues. Covariance matrix for each correlated contacts are calculated using Equation 2,

$$C_{i,j;k,l} = \langle (u_{ij} - U_{ij})(u_{kl} - U_{kl}) \rangle \tag{2}$$

where the mean contact U_{ij} and U_{kl} is used for residues i, j, k, and l contacts. The last steps of CAMERRA calculate the principal components of the contacts. These steps required Basic Linear Algebra subprograms, lblas (version 3.8.0), and Linear Algebra PACKage libraries, LAPACK (version 3.8.0). BLAS and LAPACK can be accessed in this website http://www.netlib.org/.(*58*, *59*) Subsequently, principal components, representing the collective modes of the contacts, were identified from the covariance matrix. Visualizations of corresponding contact dynamics were done using VMD.(*60*)

4 Acknowledgement

We acknowledge the Department of Science and Technology-Advanced Science and Technology Institute CoARE Facility and the UP Diliman College of Science Computational Science Research Center (CSRC) for the computing resources. We thank Christian O. Matira of the DOST-ASTI for the technical support with the Saliksik HPC. This study was funded by the Department of Agriculture-BIOTECH Program (Grant: DABIOTECH - R1605). We thank Prof. Aaron Joseph L. Villaraza, Prof. Gil C. Claudio, and Prof. Eizadora T. Yu for their

technical advice on the improvement of this study. We also thank Jackie Pugay and Maurice Franklin de Jesus for their editorial assistance.

5 Author Contributions

R.B.N. and M.K.E.B designed the experiment. M.K.E.B. performed MD simulations and analyses. R.B.N. and M.K.E.B wrote the manuscript.

6 Notes

The authors declare no competing interests.

References

1. Thal, D. M., Glukhova, A., Sexton, P. M., and Christopoulos, A. (2018) Structural insights into G-protein-coupled receptor allostery. *Nature 559*, 45.

2. Motlagh, H. N., Wrabl, J. O., Li, J., and Hilser, V. J. (2014) The ensemble nature of allostery. *Nature 508*, 331.

3. Dror, R. O., Green, H. F., Valant, C., Borhani, D. W., Valcourt, J. R., Pan, A. C., Arlow, D. H., Canals, M., Lane, J. R., Rahmani, R., et al. (2013) Structural basis for modulation of a G-protein-coupled receptor by allosteric drugs. *Nature 503*, 295.

4. Nussinov, R., and Tsai, C.-J. (2013) Allostery in disease and in drug discovery. *Cell 153*, 293–305.

5. Remesic, M., Hruby, V. J., Porreca, F., and Lee, Y. S. (2017) Recent advances in the realm of allosteric modulators for opioid receptors for future therapeutics. *ACS Chemical Neuroscience 8*, 1147–1158.

6. Lu, S., and Zhang, J. (2018) Small molecule allosteric modulators of G-protein-coupled receptors: drug–target interactions. *Journal of Medicinal Chemistry 62*, 24–45.

7. Lutz, P.-E., and Kieffer, B. L. (2013) Opioid receptors: Distinct roles in mood disorders. *Trends in Neurosciences 36*, 195–206.

8. Feng, Y., He, X., Yang, Y., Chao, D., H Lazarus, L., and Xia, Y. (2012) Current research on opioid receptor function. *Current Drug Targets 13*, 230–246.

9. Contet, C., Kieffer, B. L., and Befort, K. (2004) Mu opioid receptor: A gateway to drug addiction. *Current Opinion in Neurobiology 14*, 370–378.

10. Manglik, A., Lin, H., Aryal, D. K., McCorvy, J. D., Dengler, D., Corder, G., Levit, A., Kling, R. C., Bernat, V., Hübner, H., et al. (2016) Structure-based discovery of opioid analgesics with reduced side effects. *Nature 537*, 185.

11. Bohn, L. M., Lefkowitz, R. J., Gainetdinov, R. R., Peppel, K., Caron, M. G., and Lin, F.-T. (1999) Enhanced morphine analgesia in mice lacking β-arrestin 2. *Science 286*, 2495–2498.

12. Bohn, L. M., Gainetdinov, R. R., Lin, F.-T., Lefkowitz, R. J., and Caron, M. G. (2000) μ-Opioid receptor desensitization by β-arrestin-2 determines morphine tolerance but not dependence. *Nature 408*, 720.

13. Raehal, K. M., Walker, J. K., and Bohn, L. M. (2005) Morphine side effects in β-arrestin 2 knockout mice. *Journal of Pharmacology and Experimental Therapeutics 314*, 1195–1201.

14. Latorraca, N. R., Venkatakrishnan, A., and Dror, R. O. (2016) GPCR dynamics: structures in motion. *Chemical Reviews 117*, 139–155.

15. Huang, W., Manglik, A., Venkatakrishnan, A., Laeremans, T., Feinberg, E. N., Sanborn, A. L., Kato, H. E., Livingston, K. E., Thorsen, T. S., Kling, R. C., et al. (2015) Structural insights into μ-opioid receptor activation. *Nature 524*, 315.

16. Koehl, A., Hu, H., Maeda, S., Zhang, Y., Qu, Q., Paggi, J. M., Latorraca, N. R., Hilger, D., Dawson, R., Matile, H., et al. (2018) Structure of the μ-opioid receptor-G_i protein complex. *Nature* 547–552.

17. Flock, T., Ravarani, C. N., Sun, D., Venkatakrishnan, A. J., Kayikci, M., Tate, C. G., Veprintsev, D. B., and Babu, M. M. (2015) Universal allosteric mechanism for Gα activation by GPCRs. *Nature 524*, 173.

18. Oldham, W. M., and Hamm, H. E. (2008) Heterotrimeric G protein activation by G-protein-coupled receptors. *Nature Reviews Molecular Cell Biology 9*, 60.

19. Venkatakrishnan, A. J., Deupi, X., Lebon, G., Heydenreich, F. M., Flock, T., Miljus, T., Balaji, S., Bouvier, M., Veprintsev, D. B., Tate, C. G., et al. (2016) Diverse activation pathways in class A GPCRs converge near the G-protein-coupling region. *Nature 536*, 484.

20. Manglik, A., Kruse, A. C., Kobilka, T. S., Thian, F. S., Mathiesen, J. M., Sunahara, R. K., Pardo, L., Weis, W. I., Kobilka, B. K., and Granier, S. (2012) Crystal structure of the μ-opioid receptor bound to a morphinan antagonist. *Nature 485*, 321.

21. Zou, Y., Ewalt, J., and Ng, H.-L. (2019) Recent Insights from Molecular Dynamics Simulations for G Protein-Coupled Receptor Drug Discovery. *International Journal of Molecular Sciences 20*, 4237.

22. Kaserer, T., Lantero, A., Schmidhammer, H., Spetea, M., and Schuster, D. (2016) μ Opioid receptor: Novel antagonists and structural modeling. *Scientific Reports 6*, 21548.

23. Hertig, S., Latorraca, N. R., and Dror, R. O. (2016) Revealing atomic-level mechanisms of protein allostery with molecular dynamics simulations. *PLoS Computational Biology 12*, e1004746.

24. Dror, R. O., Arlow, D. H., Maragakis, P., Mildorf, T. J., Pan, A. C., Xu, H., Borhani, D. W., and Shaw, D. E. (2011) Activation mechanism of the β2-adrenergic receptor. *Proceedings of the National Academy of Sciences 108(46)*, 18684–18689.

25. Kruse, A. C., Hu, J., Pan, A. C., Arlow, D. H., Rosenbaum, D. M., Rosemond, E., Green, H. F., Liu, T., Chae, P. S., Dror, R. O., et al. (2012) Structure and dynamics of the M3 muscarinic acetylcholine receptor. *Nature 482*, 552.

26. Karami, Y., Bitard-Feildel, T., Laine, E., and Carbone, A. (2018) "Infostery" analysis of short molecular dynamics simulations identifies highly sensitive residues and predicts deleterious mutations. *Scientific Reports 8*, 1–18.

27. Trott, O., and Olson, A. J. (2010) AutoDock Vina: Improving the speed and accuracy of docking with a new scoring function, efficient optimization, and multithreading. *Journal of Computational Chemistry 31*, 455–461.

28. Neilan, C. L., Husbands, S. M., Breeden, S., Ko, M. H., Aceto, M. D., Lewis, J. W., Woods, J. H., and Traynor, J. R. (2004) Characterization of the complex morphinan derivative BU72 as a high efficacy, long-lasting mu-opioid receptor agonist. *European Journal of Pharmacology 499*, 107–116.

29. Lin, A. P., and Ko, M.-C. (2012) The therapeutic potential of nociceptin/orphanin FQ receptor agonists as analgesics without abuse liability. *ACS Chemical Neuroscience 4*, 214–224.

30. Burford, N., and Alt, A. Positive allosteric modulators and silent allosteric modulators of the Mu opioid receptor. 2017; US Patent 9,784,740.

31. Burford, N. T., Clark, M. J., Wehrman, T. S., Gerritz, S. W., Banks, M., O'Connell, J., Traynor, J. R., and Alt, A. (2013) Discovery of positive allosteric modulators and silent allosteric modulators of the μ-opioid receptor. *Proceedings of the National Academy of Sciences 110*, 10830–10835.

32. Bisignano, P., Burford, N. T., Shang, Y., Marlow, B., Livingston, K. E., Fenton, A. M., Rockwell, K., Budenholzer, L., Traynor, J. R., Gerritz, S. W., et al. (2015) Ligand-based discovery of a new scaffold for allosteric modulation of the μ-opioid receptor. *Journal of Chemical Information and Modeling 55*, 1836–1843.

33. Meng, X.-Y., Zhang, H.-X., Mezei, M., and Cui, M. (2011) Molecular docking: A powerful approach for structure-based drug discovery. *Current Computer-Aided Drug Design 7*, 146–157.

34. Johnson, Q. R., Lindsay, R. J., and Shen, T. (2018) CAMERRA: An analysis tool for the computation of conformational dynamics by evaluating residue–residue associations. *Journal of Computational Chemistry 39(20)*.

35. Johnson, Q. R., Lindsay, R. J., Nellas, R. B., Fernandez, E. J., and Shen, T. (2015) Mapping allostery through computational glycine scanning and correlation analysis of residue–residue contacts. *Biochemistry 54*, 1534–1541.

36. Clark, A. K., Wilder, J. H., Grayson, A. W., Johnson, Q. R., Lindsay, R. J., Nellas, R. B., Fernandez, E. J., and Shen, T. (2016) The promiscuity of allosteric regulation of nuclear receptors by retinoid X receptor. *The Journal of Physical Chemistry B 120*, 8338–8345.

37. Digby, G. J., Lober, R. M., Sethi, P. R., and Lambert, N. A. (2006) Some G protein heterotrimers physically dissociate in living cells. *Proceedings of the National Academy of Sciences 103*, 17789–17794.

38. Khafizov, K., Lattanzi, G., and Carloni, P. (2009) G protein inactive and active forms

investigated by simulation methods. *Proteins: Structure, Function, and Bioinformatics 75*, 919–930.

39. Weis, W. I., and Kobilka, B. K. (2018) The molecular basis of G protein–coupled receptor activation. *Annual Review of Biochemistry 87*, 897–919.

40. Sounier, R., Mas, C., Steyaert, J., Laeremans, T., Manglik, A., Huang, W., Kobilka, B. K., Déméné, H., and Granier, S. (2015) Propagation of conformational changes during μ-opioid receptor activation. *Nature 524*, 375.

41. Guo, J., and Zhou, H.-X. (2016) Protein allostery and conformational dynamics. *Chemical Reviews 116*, 6503–6515.

42. Bhattacharya, S., and Vaidehi, N. (2014) Differences in allosteric communication pipelines in the inactive and active states of a GPCR. *Biophysical Journal 107*, 422–434.

43. Bhattacharya, S., and Vaidehi, N. (2017) Mechanism of Allosteric Communication in GPCR Activation from Microsecond Scale Molecular Dynamics Simulations. *Biophysical Journal 112*, 498a–499a.

44. Phillips, J., Braun, R., Wang, W., Gumbart, J., Tajkhorshid, E., Villa, E., Chipot, C., Skeel, R., Kale, L., and Schulten, K. (2005) Scalable molecular dynamics with NAMD. *Journal of Computational Chemistry 26*, 1781–1802.

45. Lomize, M. A., Lomize, A. L., Pogozheva, I. D., and Mosberg, H. I. (2006) OPM: Orientations of proteins in membranes database. *Bioinformatics 22*, 623–625.

46. Jo, S., Kim, T., Iyer, V. G., and Im, W. (2008) CHARMM-GUI: A web-based graphical user interface for CHARMM. *Journal of Computational Chemistry 29*, 1859–1865.

47. Case, D. A., Cheatham, T. E., Darden, T., Gohlke, H., Luo, R., Merz, K. M., Onufriev, A., Simmerling, C., Wang, B., and Woods, R. J. (2005) The AMBER biomolecular simulation programs. *Journal of Computational Chemistry 26*, 1668–1688.

48. Maier, J. A., Martinez, C., Kasavajhala, K., Wickstrom, L., Hauser, K. E., and Simmerling, C. (2015) ff14SB: improving the accuracy of protein side chain and backbone parameters from ff99SB. *Journal of Chemical Theory and Computation 11*, 3696–3713.

49. Price, D. J., and Brooks III, C. L. (2004) A modified TIP3P water potential for simulation with Ewald summation. *The Journal of Chemical Physics 121*, 10096–10103.

50. Dickson, C. J., Madej, B. D., Skjevik, Å. A., Betz, R. M., Teigen, K., Gould, I. R., and Walker, R. C. (2014) Lipid14: The AMBER lipid force field. *Journal of Chemical Theory and Computation 10*, 865–879.

51. Wang, J., Wolf, R. M., Caldwell, J. W., Kollman, P. A., and Case, D. A. (2004) Development and testing of a general AMBER force field. *Journal of Computational Chemistry 25*, 1157–1174.

52. Wang, J., Wang, W., Kollman, P. A., and Case, D. A. (2001) Antechamber: An accessory software package for molecular mechanical calculations. *Journal of American Chemical Society 222*, U403.

53. Darden, T., York, D., and Pedersen, L. (1993) Particle mesh Ewald An N log N method for Ewald sums in large systems. *The Journal of Chemical Physics 98*, 10089–10092.

54. Pastor, R. W., Brooks, B. R., and Szabo, A. (1988) An analysis of the accuracy of Langevin and molecular dynamics algorithms. *Molecular Physics 65*, 1409–1419.

55. Feller, S. E., Zhang, Y., Pastor, R. W., and Brooks, B. R. (1995) Constant pressure molecular dynamics simulation: the Langevin piston method. *The Journal of Chemical Physics 103*, 4613–4621.

56. Martyna, G. J., Tobias, D. J., and Klein, M. L. (1994) Constant pressure molecular dynamics algorithms. *The Journal of Chemical Physics 101*, 4177–4189.

57. Roe, D. R., and Cheatham III, T. E. (2013) PTRAJ and CPPTRAJ: Software for processing and analysis of molecular dynamics trajectory data. *Journal of Chemical Theory and Computation 9*, 3084–3095.

58. Dongarra, J. J., Du Croz, J., Hammarling, S., and Hanson, R. J. (1988) An extended set of FORTRAN basic linear algebra subprograms. *ACM Transactions on Mathematical Software (TOMS) 14*, 1–17.

59. Anderson, E., Bai, Z., Dongarra, J., Greenbaum, A., McKenney, A., Du Croz, J., Hammarling, S., Demmel, J., Bischof, C., and Sorensen, D. LAPACK: A portable linear algebra library for high-performance computers. Proceedings of the 1990 ACM/IEEE conference on Supercomputing. 1990; pp 2–11.

60. Humphrey, W., Dalke, A., and Schulten, K. (1996) VMD: Visual Molecular Dynamics. *Journal of Molecular Graphics 14*, 33–38.

Table 1: μOR glycine mutants effects to PC 2 values.

PC 2 values	**Mutants**
Positive	Native, W69G, V79G, I80G, T154G, V172G, I232G, V236G, W254G, and Y262G
Negative	F59G, Q60G, D83G, Y84G, M87G, L155G, H233G, and I258G

The corresponding PC 2 versus PC 1 was projected in Figure 10.

Table 2: BU72-μOR polar interactions based from PDB ID 5C1M.

6DDE residues	**Equivalent 5C1M residues**	**PC 2 observations**
D83	D147	Negative-shifting
Y84	Y148	Negative-shifting
H233	H297	Negative-shifting
Y262	Y326	No significant shifting

Table 3: Other BU72-μOR proximal intermolecular interactions.

6DDE residues	**Equivalent 5C1M residues**	**PC 2 observations**
V79	V143	No significant shifting
M87	M151	Negative-shifting
V172	V236	No significant shifting
I232	I296	No significant shifting
V236	V300	No significant shifting
W254	W318	No significant shifting
I258	I322	Negative-shifting
Y262	Y326	No significant shifting

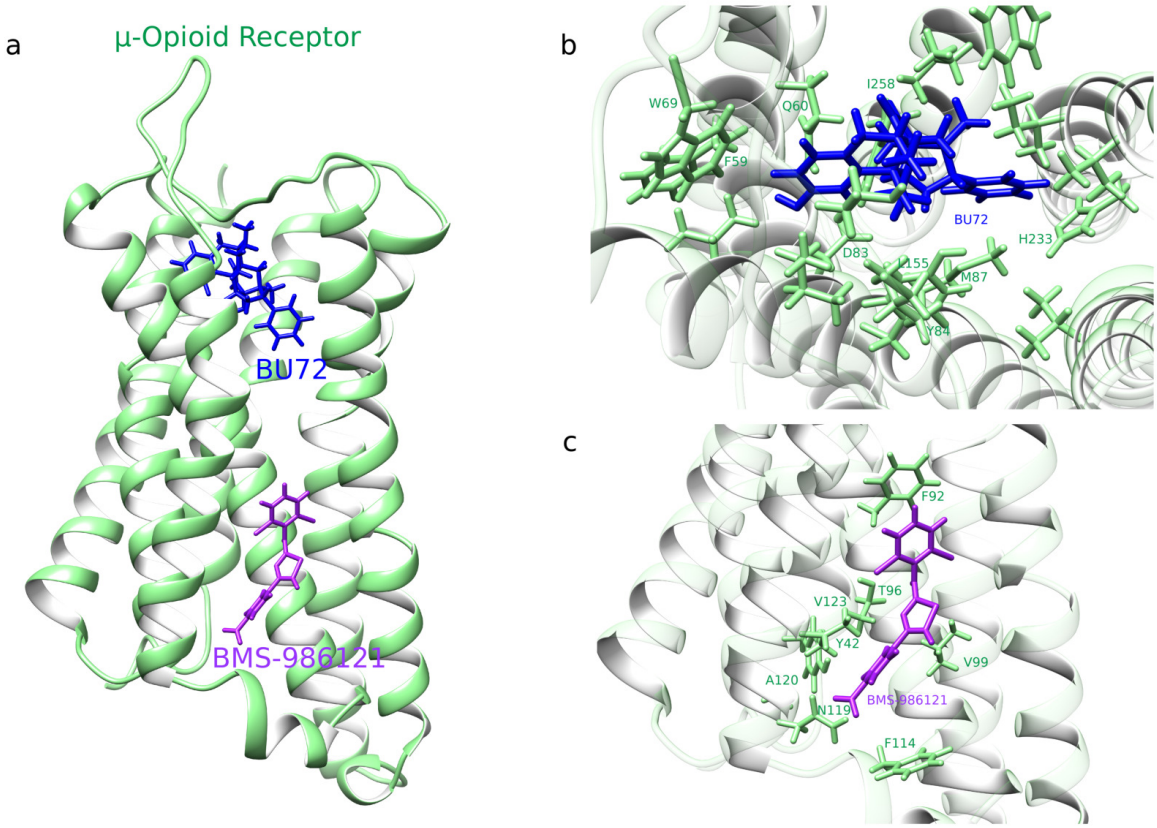

Figure 1: μOR, BU72, and BMS-986121 complex. (a) Binding pose of ligand BU72 (blue) and BMS-986121 (purple) inside μOR. Close interacting residues of μOR side chains (green stick model) with (b) BU72 and (c) BMS-986121.

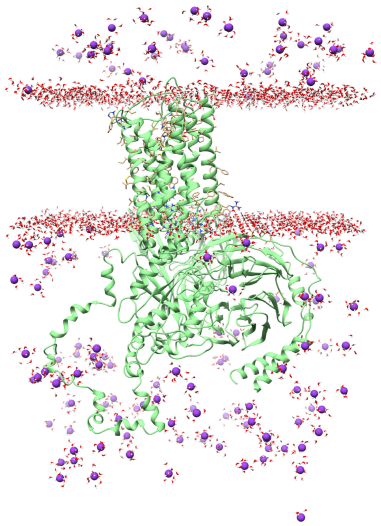

Figure 2: Molecular dynamics simulations of μOR-G protein complex. Structure of the complex was derived from PDB ID 6DDE.(*16*)

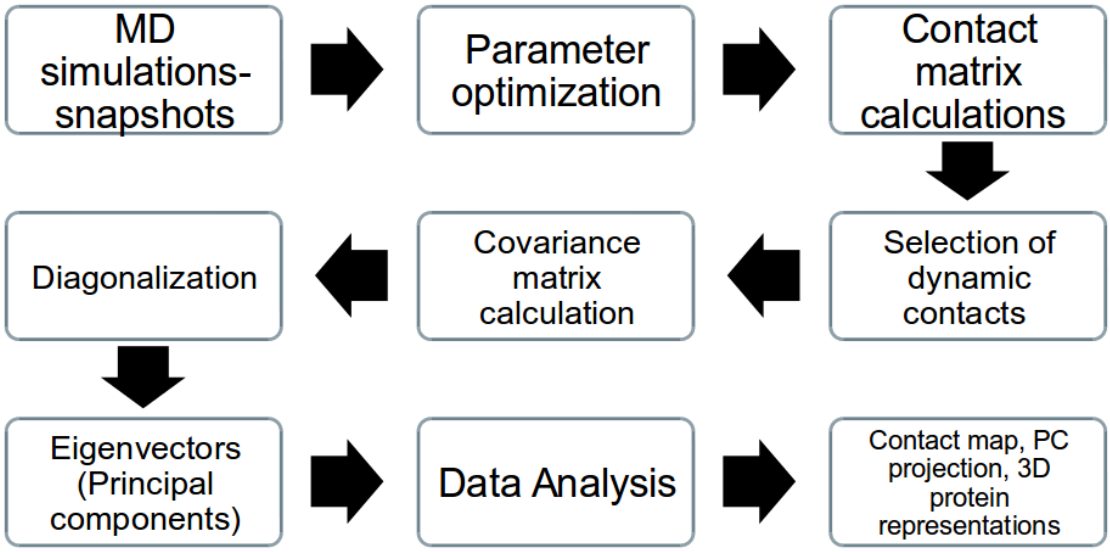

Figure 3: CAMERRA method algorithm and data analysis adapted from Johnson, et al. (*34*)

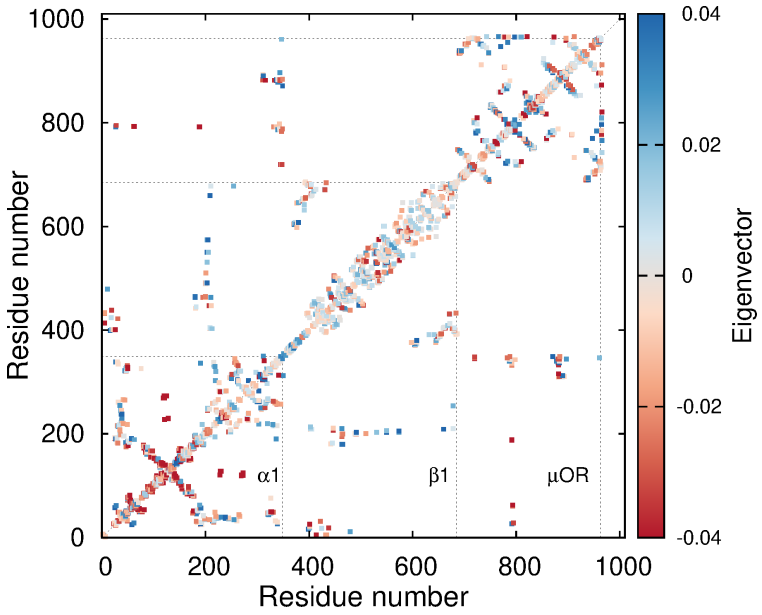

Figure 4: Potential PAM BMS-986121 and μOR G protein complex residue-residue contact map. Residue numbers are sequenced from α1-, β1-G proteins, to μOR. Intra- and interprotein contacts are separated by dashes.

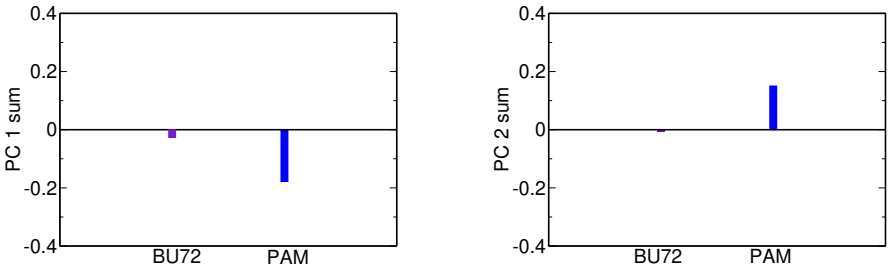

Figure 5: Potential PAM BMS-986121 and agonist BU72 PC 1 and 2 sum. Negative cooperativity and anticooperativity was observed in PC 1 and PC 2, respectively.

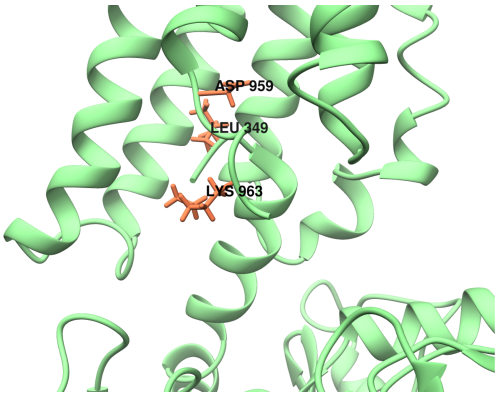

Figure 6: Interprotein contacts between μOR and α1 G protein residues.

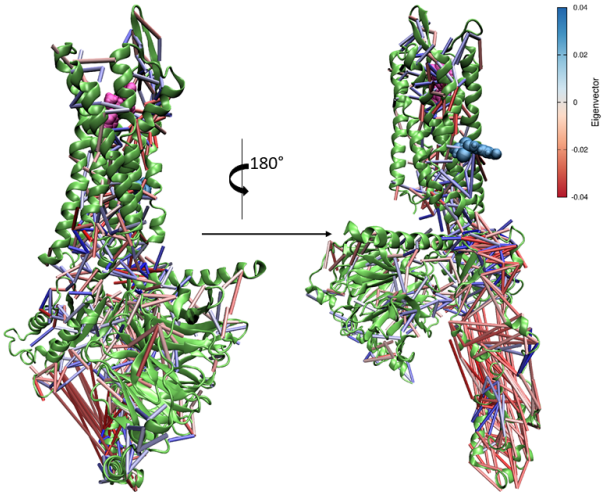

Figure 7: Potential PAM-μOR-G protein residue-residue contacts PC 1.

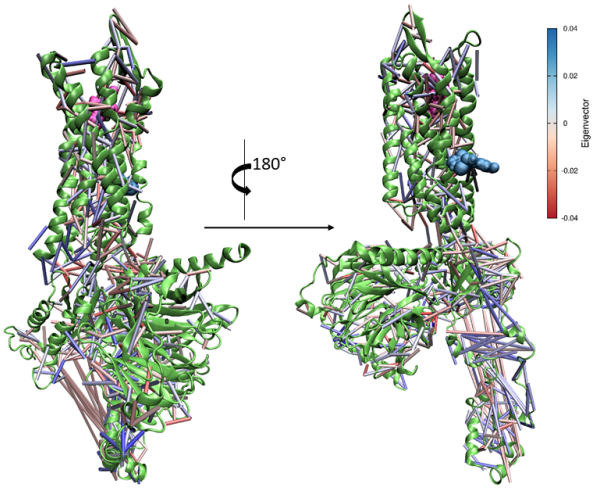

Figure 8: Potential PAM-μOR-G protein residue-residue contacts PC 2.

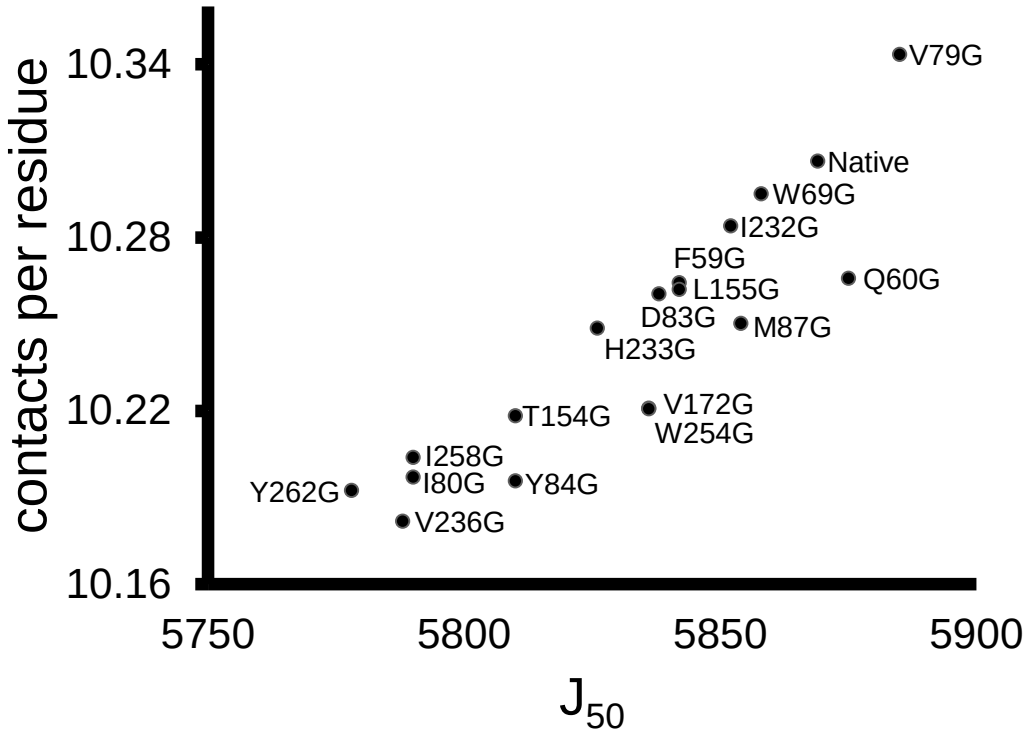

Figure 9: Number of contacts versus J_{50} for PAM-μOR-G-protein complex Native and Glycine mutants.

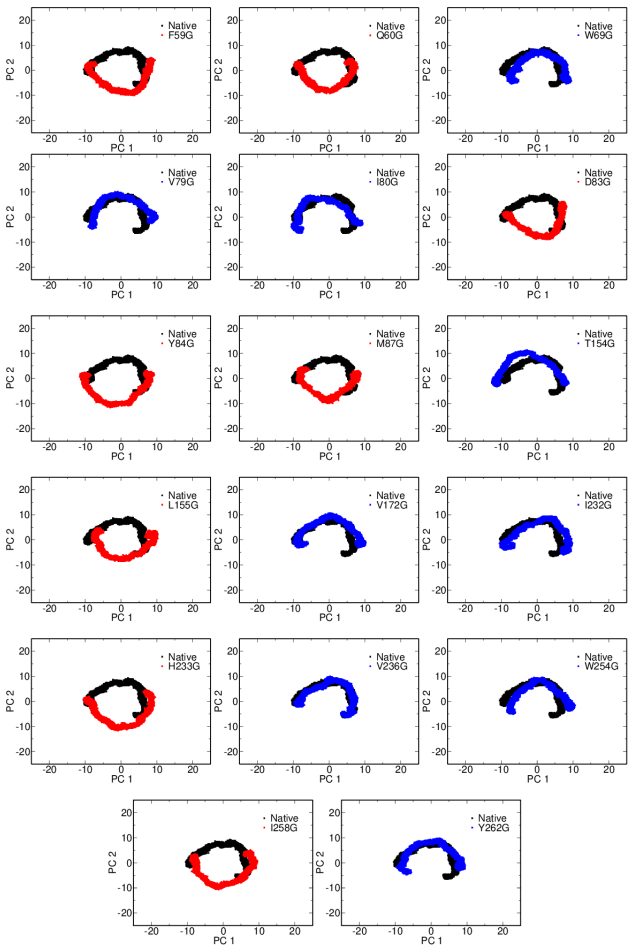

Figure 10: Principal components 1 and 2 projection at different μOR glycine mutants. Native PC points are all colored in black. Mutants PC points are colored according to their PC 2 values, positive (blue) and negative (red).

In silico Insights on the Allosteric Modulation of the μ-Opioid Receptor and G protein Complex in the Presence of Agonist Ligand BU72 and Positive Allosteric Modulator BMS-986121

Mac Kevin E. Braza and Ricky B. Nellas*

Institute of Chemistry, College of Science, University of the Philippines Diliman, Quezon City, 1101, Philippines

E-mail: rbnellas@up.edu.ph

Supplementary Information

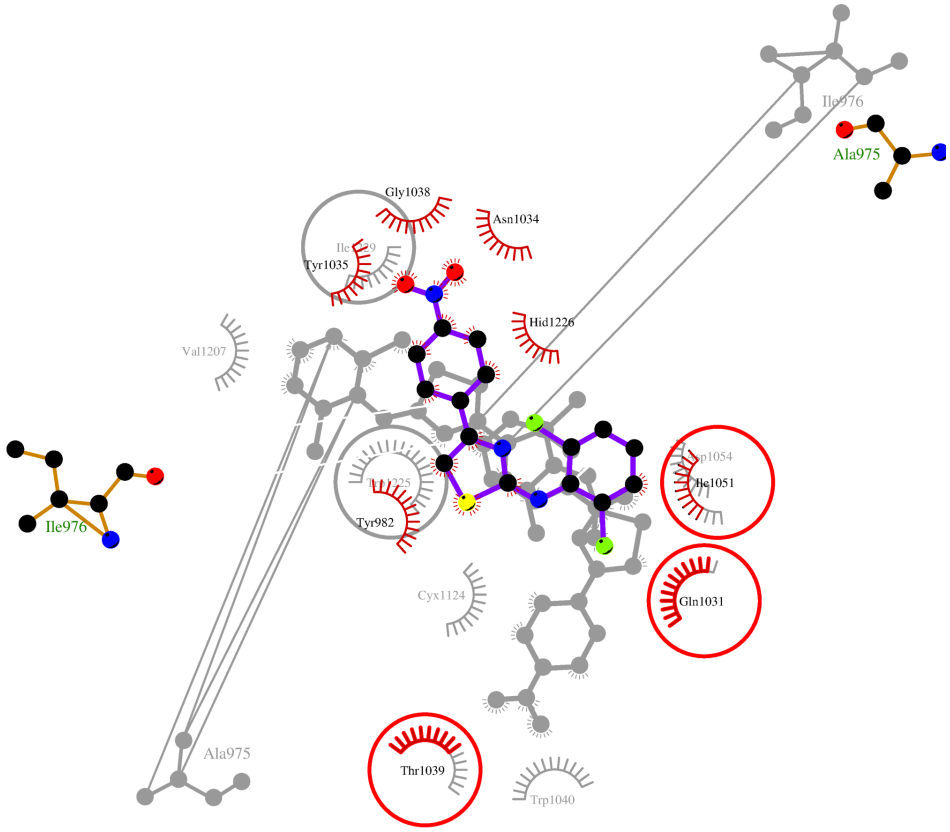

Supplementary Figure 1: μ-OR close interacting residues with PAM BMS-986121. Equivalent residues are encircled in red.

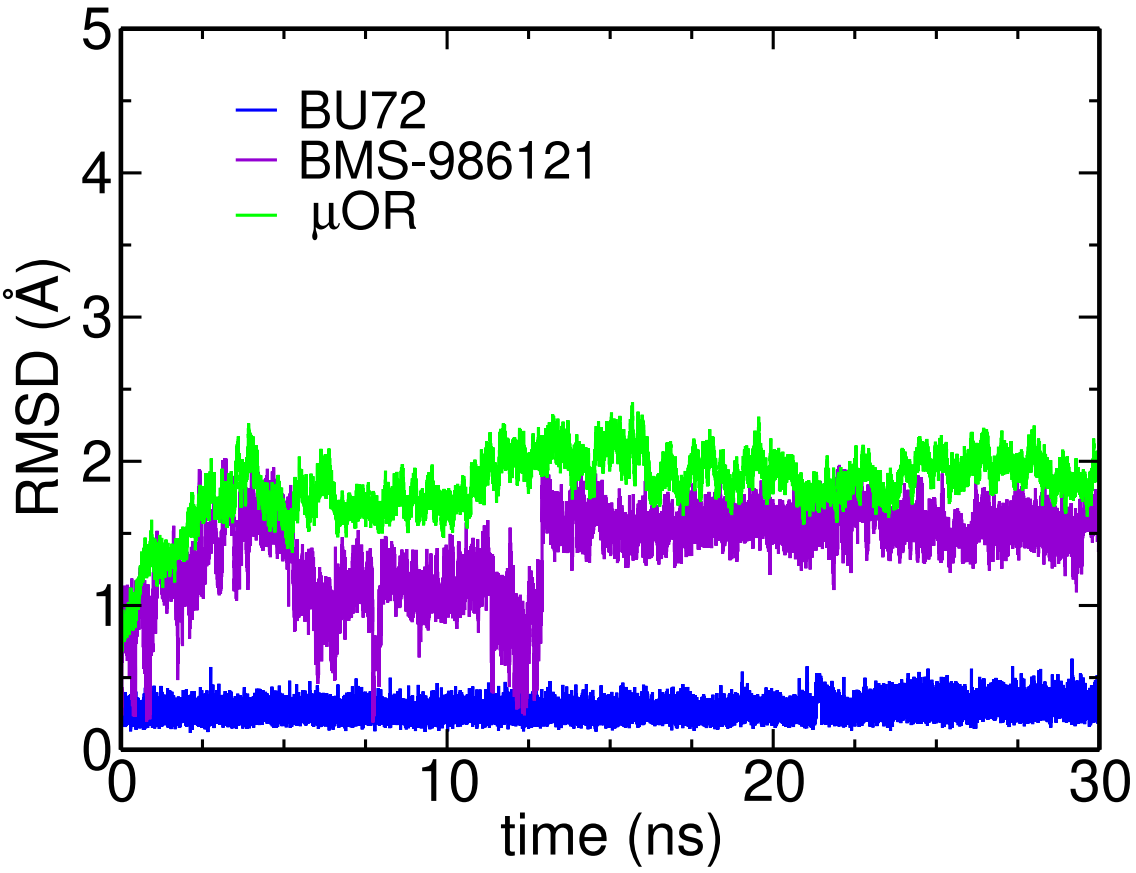

Supplementary Figure 2: Root-mean square deviation (RMSD) for ligand BU72, PAM BMS-986121, and μ-OR. Ligands' RMSD showed that the binding poses are stable.